Corrected TOGA COARE Sounding Humidity Data: Impact on Diagnosed Properties of Convection and Climate over the Warm Pool

PAUL E. CIESIELSKI AND RICHARD H. JOHNSON

Department of Atmospheric Science, Colorado State University, Fort Collins, Colorado

PATRICK T. HAERTEL

CIRES, University of Colorado, NOAA Aeronomy Laboratory, Boulder, Colorado

JUNHONG WANG

NCAR/ATD, Boulder, Colorado

(Manuscript received 11 October 2002, in final form 14 February 2003)

ABSTRACT

This study reports on the humidity corrections in the Tropical Ocean Global Atmosphere (TOGA) Coupled Ocean–Atmosphere Response Experiment (COARE) upper-air sounding dataset and their impact on diagnosed properties of convection and climate over the warm pool. During COARE, sounding data were collected from 29 sites with Vaisala-manufactured systems and 13 sites with VIZ-manufactured systems. A recent publication has documented the characteristics of the humidity errors at the Vaisala sites and a procedure to correct them. This study extends that work by describing the nature of the VIZ humidity errors and their correction scheme. The corrections, which are largest in lower-tropospheric levels, generally increase the moisture in the Vaisala sondes and decrease it in the VIZ sondes.

Use of the corrected humidity data gives a much different perspective on the characteristics of convection during COARE. For example, application of a simple cloud model shows that the peak in convective mass flux shifts from about 8°N with the uncorrected data to just south of the equator with corrected data, which agrees better with the diagnosed vertical motion and observed rainfall. Also, with uncorrected data the difference in mean convective available potential energy (CAPE) between Vaisala and VIZ sites is over 700 J kg^{-1}; with the correction, both CAPEs are around ~1300 J kg^{-1}, which is consistent with a generally uniform warm pool SST field. These results suggest that the intensity and location of convection would differ significantly in model simulations with humidity-corrected data, and that the difficulties which the reanalysis products had in reproducing the observed rainfall during COARE may be due to the sonde humidity biases.

The humidity-corrected data appear to have a beneficial impact on budget-derived estimates of rainfall and radiative heating rate, such that revised estimates show better agreement with those from independent sources.

1. Introduction

Over the past decade, atmospheric sounding data from the 1992–93 Tropical Ocean Global Atmosphere (TOGA) Coupled Ocean–Atmosphere Response Experiment (COARE; Webster and Lukas 1992) have been used extensively to study atmospheric and oceanic processes and their interactions over the western Pacific warm pool. However, shortly after the field phase of the experiment it became apparent that the sounding systems used in the COARE, a combination of Vaisala- and VIZ-manufactured systems, exhibited a variety of humidity errors. Lucas and Zipser (2000) noted unrealistically small values of convective available potential energy (CAPE) at many of the Integrated Sounding System (ISS) sites, where Vaisala-H humidity sensors were used, and concluded that these sensors displayed a dry bias (~5% in relative humidity) in the lower troposphere. They developed a correction algorithm for the Vaisala humidity data based on independent observations of surface humidity and their differences from sounding-determined mixed-layer mean values. Without the corrections, large horizontal gradients of low-level moisture over regions of nearly uniform sea surface temperature were observed, with CAPE varying by a factor of 2.5 over the COARE Intensive Flux Array (IFA; Zipser and Johnson 1998). After corrections, a more homogeneous horizontal distribution of humidity over the IFA was achieved.

Recently, Wang et al. (2002) investigated the humid-

Corresponding author address: Paul E. Ciesielski, Department of Atmospheric Science, Colorado State University, Fort Collins, CO 80523.
E-mail: paulc@atmos.colostate.edu

ity errors in the Vaisala systems used in COARE and developed a procedure for correcting them. Guichard et al. (2000a) studied the impact of the errors for one site (R/V *Moana Wave*) and found that after application of the humidity corrections, the atmosphere exhibited more realistic values of CAPE and convective inhibition (CIN), comparable to those determined from aircraft observations. They also found an important effect of the corrected moisture fields on the surface radiative budget. It is worth emphasizing that these humidity corrections for the Vaisala systems are not unique to the COARE region, but apply to operational systems used throughout the world. Humidity biases associated with the wide variety of operational sounding systems and their changes with time have important implications with regard to the accurate assessment of climate water vapor feedbacks (Elliott and Gaffen 1991; Gutzler 1993; Soden and Lanzante 1996; Spencer and Braswell 1997).

In contrast, evidence from the VIZ humidity observations, which were taken at stations in Indonesia and in the Caroline and Marshall Islands around 10°N, revealed a moist bias in the lower troposphere (Johnson and Ciesielski 2000), consistent with earlier findings for VIZ systems elsewhere by Wade and Schwartz (1993). Johnson and Ciesielski suggested that differences in the north–south distribution of precipitation over the warm pool during COARE between observations and operational center model reanalyses may be attributable to the combined humidity errors of the Vaisala and VIZ systems.

Considering the crucial role that water vapor plays in the climate system and the extensive past, present, and future use of the COARE sounding dataset, we are motivated in this paper to explore humidity biases for COARE soundings in greater detail and over a larger area than in past studies, and examine their impacts on various analyses over the warm pool. This is done by using corrected humidity data from all Vaisala and VIZ sites in and near the COARE Large-Scale Array (LSA), where the corrections to the Vaisala humidities are described in Wang et al. (2002) and a procedure for correcting the VIZ humidities is described briefly in section 2. The magnitudes of the humidity corrections are examined in section 3 with an emphasis on the boundary layer where the corrections are a maximum. The influence of humidity-corrected (HC) data on convection is studied in section 4. In particular, changes in CAPE and CIN over the warm pool are examined. Recognizing the critical role of low- and midlevel moisture in regulating deep convection (e.g., Crook 1996; Nicholls et al. 1988; Raymond 1995; Lucas et al. 2000), the resulting impacts on cloud detrainment and mass flux profiles are analyzed with a one-dimensional cloud model.

In section 5 an objective gridded analysis is used to investigate the impact of the HC data on atmospheric heat and moisture budgets on various time and space scales. Using the Lucas and Zipser (2000) corrected humidity data at the ISS sites in a preliminary sensitivity test, Johnson and Ciesielski (2000) suggested that a HC dataset would have only a small effect on the COARE-mean diagnosed rainfall and radiative heating rates ($<$3% and 10%, respectively). Using the HC dataset, we will show that the impact of the corrections on budget-diagnosed fields is considerably larger than originally thought.

Section 6 examines the effects of the HC data on forcing fields (i.e., large-scale tendencies of temperature and moisture) for cloud-resolving models (CRMs) and single-column models (SCMs). Emanuel and Živković-Rothman (1999), Wu et al. (2000) and Guichard et al. (2000b) have performed a moist enthalpy analysis for the COARE period to evaluate the quality of the large-scale forcing data computed with uncorrected humidity data and have concluded that problems exist with this forcing dataset. We perform a similar enthalpy analysis, which shows that use of HC data could potentially have a beneficial impact on long-term model integrations.

In section 7 we consider how the corrected humidities affect the diurnal cycle of budget-derived quantities. Finally, our major findings are summarized in section 8 with a description of how to access the various humidity-corrected data products.

2. Nature of humidity corrections and data sources

Figure 1 shows the location and radiosonde system type for the sounding sites in the vicinity of the COARE LSA. Also shown in this map are the Outer Sounding Array (OSA) and the IFA. During the COARE intensive observation period (IOP; 1 November 1992–28 February 1993) sites within these two arrays typically had four sonde launches per day, while outside the OSA sites had only two launches per day. Three types of sonde system were used in COARE: the Vaisala RS80_H (VaH) and its predecessor the RS80_A (VaA), which have capacitive humidity sensors, and the VIZ system, which has a resistance-type humidity sensor. The VaH systems, deployed at the ISS sites, were used at the majority of the IFA sites, while the VIZ systems were used primarily at sites around 10°N. Although the COARE sounding domain extends to 100°E and includes 43 sounding sites,[1] this paper will focus on the data from the 29 sounding sites shown in Fig. 1 and for the period of the COARE IOP.

A cooperative effort between the Vaisala Corporation and National Center for Atmospheric Research/Atmospheric Technology Division (NCAR/ATD) led to the identification of six different humidity errors in the Vaisala sonde system. A detailed description of these six errors (listed in Table 1) and the procedure to correct them is given by Wang et al. (2002). For temperatures above −20°C, the most serious error was due to chem-

[1] The sonde data from Davao in the Philippines had only wind observations.

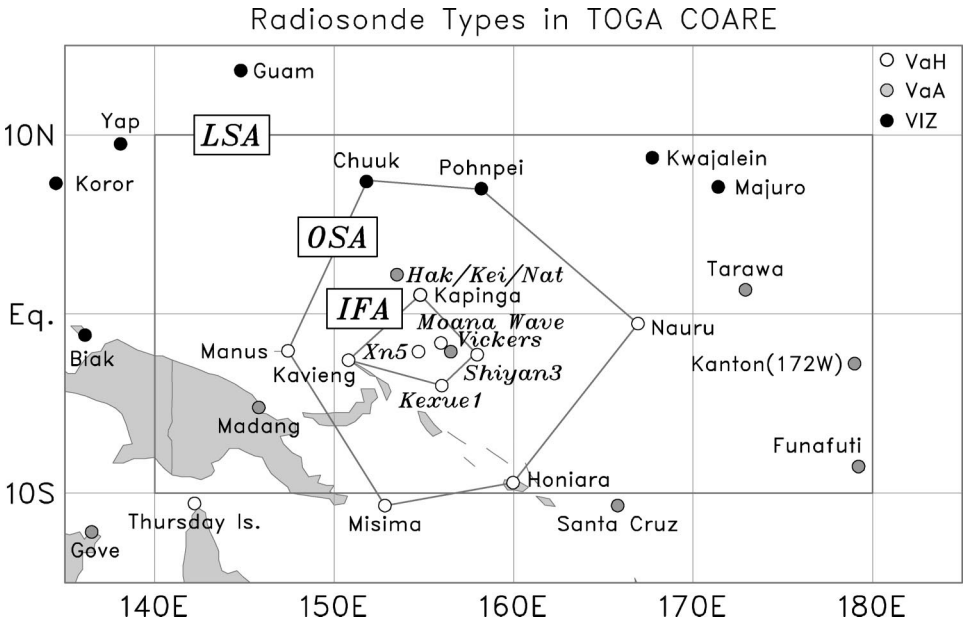

FIG. 1. Map showing the various types of radiosonde sensors used during TOGA COARE. Also shown are the sounding arrays in TOGA COARE: the Large-scale Sounding Array (LSA), the Outer Sounding Array (OSA), and the Intensive Flux Array (IFA). The locations of the research vessels, which are shown in italics, represent their nominal positions. The Japanese ships (*Hak*/*Kei*/*Nat*) shown to the north of the IFA actually cruised in and out of the IFA.

ical contamination of the humidity sensor, a dielectric polymer, by aging packing material. The contamination error reduced the ability of the sensor to absorb water vapor resulting in a dry bias, which increased with sonde age and relative humidity (RH). This error is larger in VaH sondes, such that for a 1-yr-old VaH sonde at saturation the RH is about 10% too low. For temperatures below -20°C an error referred to as the temperature dependent (TD) error dominates. Occurring in both VaH and VaA sondes type, this error resulted from approximating the actual nonlinear temperature dependence of the humidity sensor by a linear function. The TD error, which is larger in the VaA sondes, increases with decreasing temperature. Applying an algorithm to correct for the six errors listed in Table 1 to both VaA and VaH sondes, NCAR/ATD corrected the humidity data in 8129 sondes at 29 Vaisala sites. After the corrections were made, each sonde was visually inspected and ''unreasonable'' humidity data values generated by the correction procedure were changed to missing values.

TABLE 1. Errors identified by Wang et al. (2002) in Vaisala sondes.

Error type	Notes
Chemical contamination	Largest error in VaH sondes
Temperature dependence	Largest error for $T < -20$°C
Basic calibration	
Sensor arm heating	Affects daytime sondes only
Ground check	
Sensor aging	

Scientists at NCAR/ATD also examined the humidity errors that occurred at the VIZ sites. They found that the VIZ sensor was characterized by a low-level (below 750 hPa) moist bias, which was considerably larger in the nighttime sondes. The moist bias in the daytime sondes may have been reduced by daytime heating of the VIZ hygristor. In addition to this low-level moist bias, a significant midlevel (700–300 hPa) dry bias relative to the mean Vaisala profiles in Fig. 2 is observed in the VIZ data. While some of the difference may be attributed to real horizontal variability, similar instrument biases were observed in the Tropical Rainfall Measuring Mission Large Scale Biosphere–Atmosphere Experiment in Amazonia (TRMM-LBA) based on 19 sonde launches taken at Abracos, Brazil, where the sonde packages carried both sensor types (J. Halverson 2001, personal communication). Ongoing efforts are attempting to understand the midlevel humidity differences between the VIZ and Vaisala sensors.

Although the reasons for the biases in the VIZ sensors are still uncertain, NCAR/ATD developed a correction procedure, based on a modified hygristor response curve (suggested by Wade and Schwartz 1993). This procedure, which reduces the low-level moist bias by as much as 4%, was applied to correct 3411 VIZ soundings at 13 sites. As a final check of the correction procedure, the humidity data from each sonde were visually inspected in a skew-*T* format and obvious glitches were set to missing values. While the current VIZ correction procedure is incomplete, specifically lacking a correc-

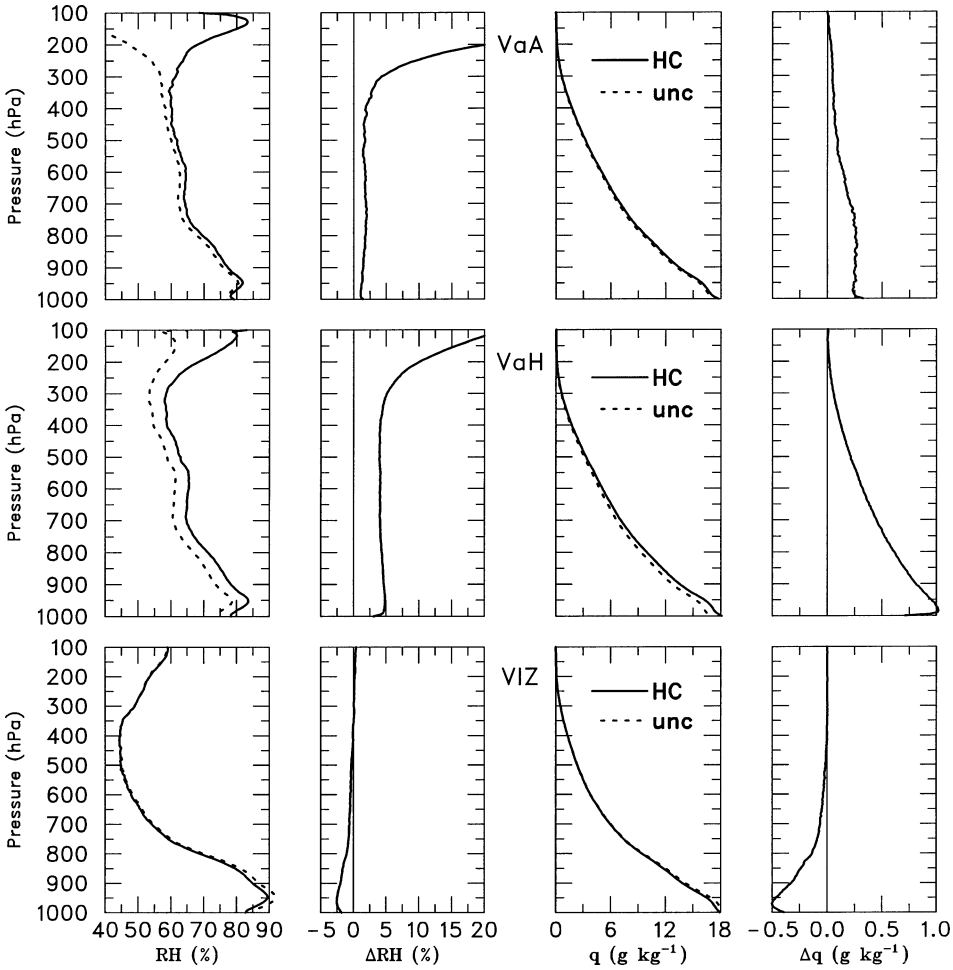

FIG. 2. Magnitude of humidity correction for various sensor types: (top) VaA, (middle) VaH, and (bottom) VIZ. Curves show mean vertical profiles and their difference [Δ = corrected (HC) minus uncorrected (unc)] for relative humidity with respect to ice (left columns) and specific humidity (right columns).

tion above 700 hPa, its reduction of the lower-tropospheric moist bias appears reasonable, and thus useful for our present purpose.

In this study the impacts of the humidity corrections on various analyses are examined relative to an ''uncorrected'' humidity dataset. The uncorrected upper-air dataset (Loeher et al. 1996) was obtained from Joint Office for Science Support (JOSS) TOGA COARE web site. As pointed out by Wang et al. (2002), this earlier version of the upper-air sonde dataset actually contains an erroneous correction for the sensor arm heating (SAH) error listed in Table 1. Based on their analyses Wang et al. develop a revised correction procedure for the SAH error. The corrected humidity upper-air Vaisala and VIZ sonde data were obtained from NCAR/ATD.[2] For more accurate analysis of atmospheric budgets, a merged dataset of rawinsonde and profiler winds at the ISS sites (Ciesielski et al. 1997) was used in this present study.

For computation of atmospheric budgets, fields of surface evaporation E and sensible heat flux S are based on National Centers for Environmental Prediction (NCEP) reanalysis values adjusted towards an IFA-mean value representing the average of four buoys in or near the IFA (Lin and Johnson 1996).

For comparison to budget-derived rainfall, satellite estimates of rainfall for the COARE domain were obtained from two sources: the Climate Prediction Center (CPC) Merged Analysis of Precipitation (CMAP) analysis of Xie and Arkin (1997), and the mixed rainfall algorithm of Curry et al. (1999). The CMAP analysis, available on a monthly basis at 2.5° resolution, represents a merger of rain gauge with a variety of infrared (IR) and microwave satellite estimates. The Curry analysis, at 3-h and 0.5° resolution over the IFA domain,

[2] The Vaisala humidity-corrected sonde data in their native vertical resolution were made available at JOSS during spring 2002; due to limitations in the VIZ humidity corrections and pending further analyses, the VIZ HC sonde data have not been released to JOSS.

TABLE 2. Impact of corrected humidity data on convective parameters computed from sondes launched from the sites shown in Fig. 1. Here, Δ refers to the change in a parameter as a result of using the corrected humidity data; unc = uncorrected, cor = corrected. Number of sondes is shown in parentheses after sonde type.

	VaA sonde (1218)			VaH sonde (3891)			VIZ sonde (2724)		
Parameter	unc	cor	Δ	unc	cor	Δ	unc	cor	Δ
CAPE (J kg^{-1})	921	961	(+40)	822	1272	(+450)	1609	1315	(−294)
CIN (J kg^{-1})	−101	−65	(+36)	−139	−43	(+96)	−16	−22	(−6)
PW (kg m^{-2})	50.5	51.4	(+0.9)	49.1	52.1	(+3.0)	48.4	47.6	(−0.8)
LCL (hPa)	923	925	(+2)	918	930	(+12)	950	944	(−6)
LNB (hPa)	162	157	(−5)	172	157	(−17)	145	155	(+10)

combines visible and IR data from geostationary satellites with microwave rainfall retrievals from polar-orbiting satellites.

3. Magnitude of humidity correction

Figure 2 shows the magnitude of the humidity correction for the various sensor types used in the COARE domain in terms of relative humidity (RH, left-hand side) and specific humidity (q, right-hand side). These mean profiles were constructed by averaging individual sondes at 5-hPa resolution from all the sites shown in Fig. 1. The number of sondes that entered into the mean for each sensor type are listed in Table 2. In the VaA sondes, the correction increases the mean RH about 1%–2% below 300 hPa with a dramatic increase in the correction above this level to a maximum of over 50% (not shown) near 100 hPa. In terms of specific humidity, the correction moistens the troposphere below 700 hPa about 0.25 g kg^{-1} with a gradual decrease above this level. In the VaH sondes, the HC data increases the mean RH about 5% below 300 hPa. Above this level the correction increases to a maximum of about 20% near 100 hPa. In terms of specific humidity the correction moistens the boundary layer about 1 g kg^{-1} with a gradual decrease in the correction with height. In the VIZ sondes, the correction has little or no impact above 700 hPa. Below this level the correction decreases mean RH from 2%–3%, which translates into a 0.5 g kg^{-1} decrease in specific humidity at 950 hPa.

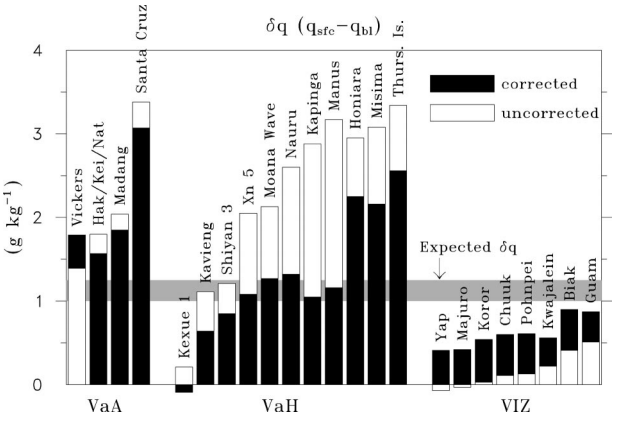

FIG. 3. Difference between the surface and boundary layer mean specific humidity, δq, for several of the sounding sites shown in Fig. 1 computed with uncorrected data (top of white bar except for Yap and Majuro, which have a negative uncorrected δq) and humidity corrected (HC) data (top of black bar expect for *Kexue 1*, in which case the corrected data results in a negative δq). The horizontal gray bar denotes the expected range for δq in the warm pool region. Sites are grouped according to sonde-sensor type: VaA, VaH, and VIZ (from left to right).

Having examined how the correction data affects humidity as a function of sensor type, we now focus on its impact in the boundary layer at individual sites. Figure 3 shows the mean specific humidity difference (δq) between the surface and boundary layer computed from sondes launched during the COARE IOP. The surface q value represents an observation from a surface-based sensor independent of the sonde, while the boundary layer value is the mean q averaged from the first point above the surface up to and including the 960-hPa level. This analysis is shown only for sites from Fig. 1 that had at least 100 soundings of good quality data in both the humidity-corrected and uncorrected dataset.[3] Results from the three Japanese ships (R/V *Hakuho-Naru*, *Keifu Maru*, *Natsushima*) that collectively launched 170 sondes in the vicinity of the IFA are considered together. In Fig. 3 the top of the white (black) bar represents the mean δq computed with uncorrected (corrected) humidity data. The only exception to this is for R/V *Kexue 1* in which the bottom of the black bar represents the corrected gradient (i.e., the corrected q gradient is negative).

Evidence from low-level COARE aircraft measurements and Monin–Obukhov similarity theory indicate that δq should be ~1.0–1.25 g kg^{-1} over the warm pool region (Zipser and Johnson 1998). While only a few sites exhibit this magnitude of δq with uncorrected data, the δq's computed with the HC data are in much better agreement with this expected value. In general, the correction acts to dry out the boundary layer of the VIZ sites (i.e., δq increases), and moistens the boundary layer of the Vaisala sites (i.e., δq decreases). The exception to this is with the R/V *Vickers*, a VaA site that showed a dry correction. At this site, young sonde age combined

[3] At the time that the uncorrected sonde data were released, many of the humidity errors in the data were still unknown such that data containing these errors were typically flagged as being of good quality.

with careful ground check corrections prior to launch yielded an original dataset that was quite accurate, and as such, humidity corrections were unnecessary. Also, the main source of humidity error at R/V *Kexue 1* was different in nature[4] from those at the other Vaisala sites resulting in a low-level moist bias at this site. The correction procedure, which was not designed to handle a moist bias at a Vaisala site, had an adverse effect upon the correction of humidity at this site. For consistency NCAR/ATD applied a similar correction procedure to all Vaisala sites. However, for the reasons stated above, uncorrected humidity data from the *Vickers* and *Kexue 1* are judged to be of better quality, so that the ''corrected'' data from these two sites are not considered further in this study.

Of the six IFA sounding sites that were present for the majority of the IOP[5] all have a corrected δq near or <1.0 g kg^{-1}, except for the *Moana Wave*, which has $\delta q = 1.3$ g kg^{-1} (Fig. 3). In studying the mixed-layer properties at four IFA sites (*Shiyan 3, Xn 5, Moana Wave,* Kapinga) with the HC dataset, Johnson et al. (2001) found that the difference between the mean lifting condensation level (LCL) and the mean mixed-layer top was ~170 m at three of the sites, the exception being the *Moana Wave* where the difference was 240 m. Since a drier boundary layer leads to a higher LCL, Johnson et al. suggested that the humidity at the *Moana Wave* was slightly undercorrected, which is consistent with its larger corrected δq in Fig. 3. Finally we note, that four Vaisala sites (Honiara, Misima, Thursday Island, and Santa Cruz) have large δq's (>2 g kg^{-1}) even with HC data. While the reason for these larger δq's is uncertain, it is worth noting that these four sites are all located on larger islands and are geographically grouped along 10°S in a region of slightly cooler SSTs (cf. Fig. 5 from Lin and Johnson 1996).

4. Impacts on diagnosed properties of convection

As noted in Fig. 2 and described earlier, the humidity corrections are a maximum in the lower troposphere. Because of the strong sensitivity of convection to the low-level thermodynamic field (e.g., Crook 1996), this section considers several ways that the HC data can affect convective properties.

Table 2 shows the impact of using the HC data on various convective parameters. These computations were done for all soundings that had good quality data over the entire depth of the troposphere and for all sites shown in Fig. 1. In this table and throughout the rest of this paper, the symbol Δ signifies the change in a quantity resulting from use of the HC data. CAPE and CIN were calculated assuming pseudo-adiabatic ascent using mean thermodynamic conditions in the lowest 50 hPa. In the VaH sondes, use of the HC data results in large changes in the mean convective parameters: CAPE increases 450 J kg^{-1}, |CIN| decreases 96 J kg^{-1}, precipitable water (PW) increases by 3 kg m^{-2}, the LCL lowers 12 hPa, and the level of neutral buoyancy (LNB) rises 22 hPa. The changes in these parameters in the VaA sondes, while in same sense but considerably smaller in magnitude, are consistent with the smaller humidity changes noted in Figs. 2 and 3. For the VIZ sondes, use of the humidity corrections, which act to dry the boundary layer, results in a CAPE decrease of ~300 J kg^{-1} and a |CIN| increase of 6 J kg^{-1}. While this ΔCIN at the VIZ sites seems small, its percentage change (~37%) is similar to that at the VaA sites. The smaller values of PW in the VIZ sondes compared to the Vaisala sondes reflects the midlevel dryness in the VIZ data.

Comparison of the mean CAPE values at the VIZ and VaH sites in Table 2 shows much better agreement when computed with the HC data, both being around 1300 J kg^{-1}. This value, being representative of sondes launched in both convectively active and suppressed periods, seems reasonable when compared with the mean CAPE value of 1471 J kg^{-1} found by LeMone et al. (1998) based on aircraft measurements in the vicinity of 20 convective systems. Also, the similar values of IOP-mean corrected CAPE at VaH and VIZ sites are consistent with the generally uniform SST field over the warm pool region.

On the basis of CAPE and CIN values in Table 2 computed with uncorrected Vaisala data, we concur with the assessment of Guichard et al. (2000a) that ''one might erroneously conclude that it is difficult to trigger deep convection over the region'' of the warm pool. However when the humidity corrections are considered in the Vaisala sondes, we observe an atmosphere ''typically near a threshold where convection is easily initiated or least maintained'' (Guichard et al. 2000a). On the other hand, the high CAPE and low CIN values observed in the uncorrected VIZ data might lead one to mistakenly conclude that the atmospheric state in the vicinity of the VIZ sites is one with almost no convective inhibition and primed for vigorous convective development.

While the analyses of CAPE and CIN emphasize the importance of low-level thermodynamic conditions in regulating convection in the warm pool region, other factors also need to be considered. Based on the similar values of humidity-corrected CAPEs that exist over the IFA (primarily from VaH sondes) and over the northern LSA (VIZ sondes), one might expect comparable convective activity and rainfall amounts in both these regions. In reality, satellite-based rainfall products for the COARE IOP, such as CMAP (Fig. 8, middle) show 50% less rainfall in the vicinity of the VIZ sites along 10°N than over the IFA. This lack of a correlation between

[4] The sondes on the *Kexue 1* were stored in a very cold, air conditioned room such that condensation formed on humidity sensors when the sondes were taken from the room resulting in the observed low-level moist bias.

[5] *Kexue 1, Shiyan 3, Xn 5, Moana Wave,* Kavieng, and Kapinga.

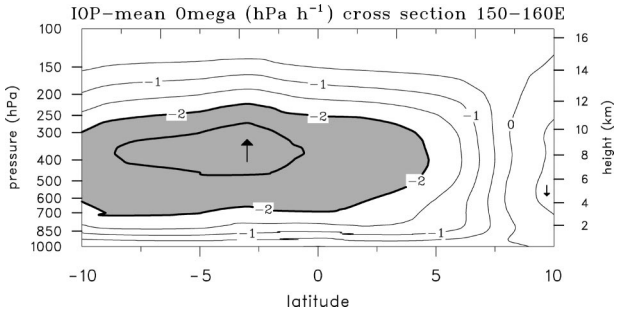

FIG. 4. IOP-mean zonally averaged omega (hPa h^{-1}) between 150° and 160°E diagnosed from objectively analyzed wind fields. Upward motion with values less than −2 hPa h^{-1} is shaded.

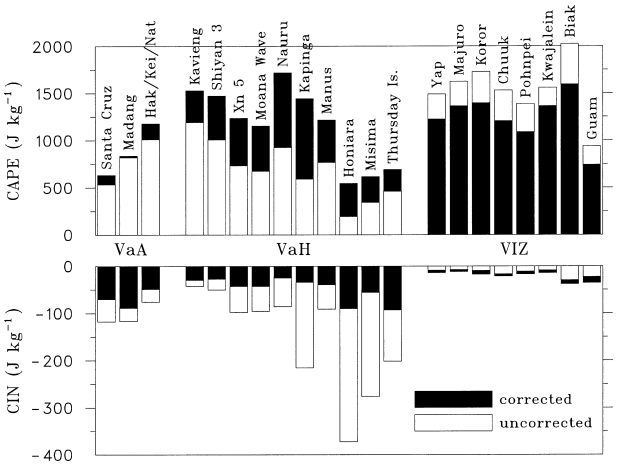

FIG. 5. (top) Mean values of CAPE at several sounding sites computed with humidity-corrected data (top of black bar) and uncorrected data (top of white bar). (bottom) Mean values of CIN computed with humidity-corrected data (bottom of black bar) and uncorrected data (bottom of white bar). Sites are grouped according to sonde-sensor type: VaA, VaH, and VIZ (from left to right).

CAPE and the rainfall pattern is consistent with previous studies (e.g., Mapes and Houze 1992; Sherwood 1999) which did not find a strong relationship between CAPE and convective development. Recent studies (e.g., Sherwood 1999; Parsons et al. 2000; Lucas et al. 2000) have found that moisture above the boundary layer plays an important role in regulating convection over the warm pool, which could explain the rainfall decrease over the northern LSA considering the the drier midtroposphere over that region (Fig. 8). Finally, it is worth emphasizing that the consistency between the satellite-observed rainfall pattern (Fig. 8) and the independently diagnosed vertical motion (Fig. 4) is worth noting. The strong coherence between these fields shows that the location of convection is strongly linked to the dynamics, as the nature of the large-scale lifting field is largely convective.

Changes in CAPE and CIN at individual sites due to the HC data are shown in Fig. 5. As one might expect, the magnitude of changes in these parameters at individual sites generally follows the magnitude of the boundary layer moisture change (δq) depicted in Fig. 3. While most sites show significant changes in CAPE and CIN due to the humidity corrections, the changes at a few VaH sites are exceptionally large. For example, at Nauru and Kapinga the mean CAPE increases over 800 J kg^{-1}, while at Kapinga, Misima, and Honiara the |CIN| decreases over 180 J kg^{-1}. These site-to-site differences in the convective parameter changes suggest that the geographical distribution of convection could be significantly different when modeled using the HC dataset.

To further explore the impact the humidity corrections on convection, we utilize the buoyancy-sorting cloud model of Raymond and Blyth (1992). This model is based on the premise that entrainment and mixing in clouds occurs as a random, highly episodic process. In this model, a parcel representing the mean properties of the 1000–950-hPa layer ascends through the troposphere up to the LNB. At each 5-hPa level the parcel mixes with environmental air with different mixing fractions ranging from 0.1 to 0.9. These diluted parcels then ascend or descend to their nearest level of neutral buoyancy with no overshooting allowed. For the results to be shown here, we assume that as the parcel ascends and water condenses, it can hold a maximum of 3 g kg^{-1} of liquid water. Above this threshold, which represents a midrange value used in Global Atmospheric Research Programme (GARP) Atlantic Tropical Experiment (GATE) simulations (Ferrier and Houze 1989), water falls out as precipitation.

The model was applied to individual sondes (both humidity-corrected and uncorrected) from seven sites for each sensor type. Model results from the individual sondes, which were required to have good thermodynamic data through the depth of the troposphere, were then averaged into mean profiles for each sensor type. The VIZ sites (2351 sondes) were between 7° and 13°N; the seven VaH sites (1979 sondes) were within 3° of the equator (see Fig. 1). In this manner, the mean profiles are representative not only of a sensor type but also of a geographical region. Unfortunately a smaller regional grouping for the VaA sites was not possible, so that the seven VaA sites (795 sondes) used were from within the LSA domain. Results from the model for the various sensor types are shown in Fig. 6 in terms of mean vertical profiles of detrainment probability and convective mass flux. The results in the left-hand side are for the case where no ice effects are included, whereas those on the right allow for ice formation, which enhances parcel buoyancy. For these latter results, the model assumes equilibrium ice processes (i.e., all water substance below 0°C is ice).

The small humidity increases in the corrected VaA sondes, depicted in Figs. 2 and 3, have little or no impact on detrainment and convective mass flux profiles. In contrast, the humidity-corrected VaH data have a significant impact on these fields with less detrainment

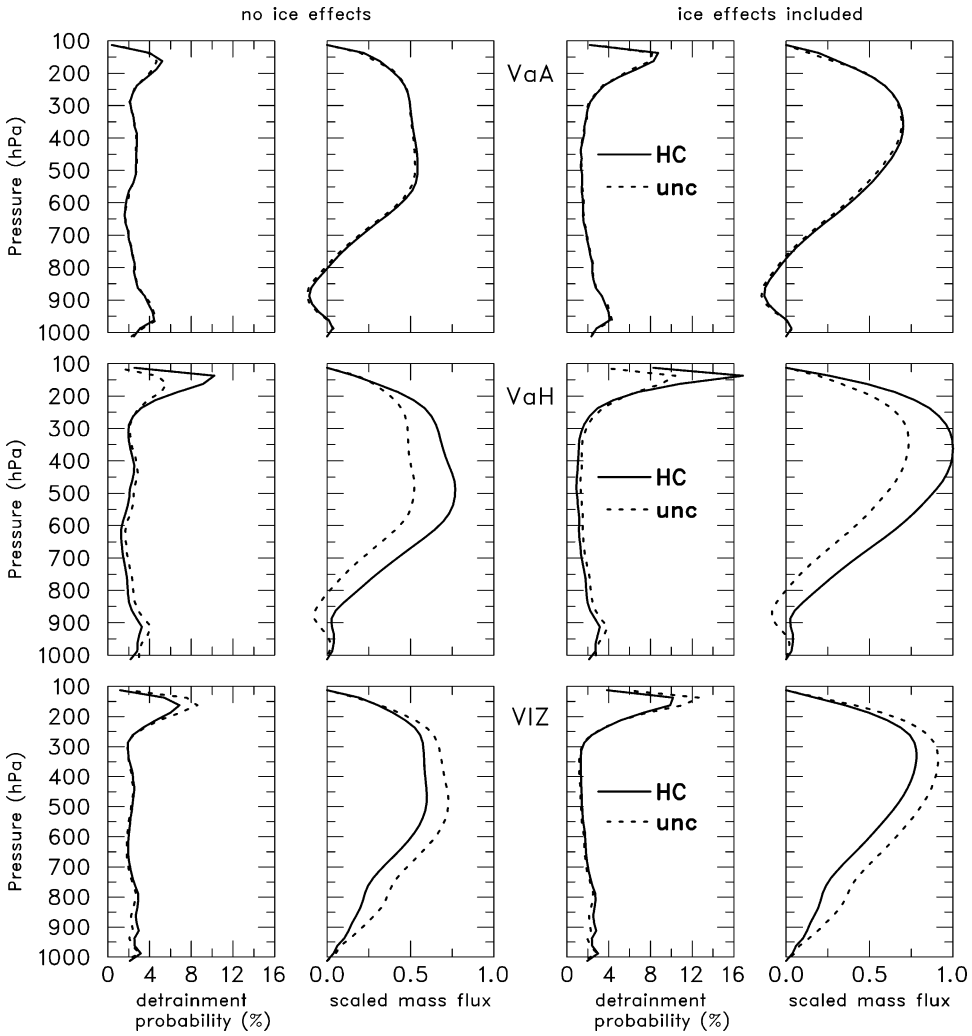

FIG. 6. Vertical mean profiles of detrainment probability and scaled convective mass flux from the Raymond–Blyth buoyancy-sorting cloud model computed with humidity-corrected data (solid line) and uncorrected data (dashed line) for the different sonde-sensor types: (top) VaA, (middle) VaH, and (bottom) VIZ. (left) Results with no ice-effects, and (right) results where ice formation is allowed. The mass flux profiles have been normalized by the largest mass flux value.

below 250 hPa compensated for by nearly twice the frequency of outflow layers above this level. In the no-ice case, there is a secondary peak in outflow layers observed near 400 hPa, presumably related to a layer of enhanced stability near the 0°C level (Johnson et al. 1996; Zuidema 1998). When ice effects are included, this secondary detrainment is no longer present as the additional latent heating due to freezing and deposition enhances buoyancy allowing more parcels to detrain at higher levels. These changes in detrainment due to the use of HC data translate into an ~30% increase in the mean convective mass flux in the 500–300-hPa layer. Using the humidity-corrected VIZ sondes results in trends in these fields that are in an opposite sense, that is, a reduction in the frequency of upper-level outflow layers corresponding to a ~15% reduction in the mean convective mass flux in the 500–300-hPa layer. Based on the IOP-mean mass flux profiles at individual sites, Fig. 7 shows a latitudinal cross section of mass flux with corrected and uncorrected data. This analysis shows that the peak in the IOP-mean mass flux shifts from about 8°N with the uncorrected data to just south of the equator with HC data, which is more consistent with the diagnosed vertical motion distribution (Fig. 4) and the observed rainfall pattern (see CMAP rainfall analysis in Fig. 8) for this period. Hence these results show that the HC data have a significant impact on the intensity and distribution of convection.

To further explore this effect, a latitudinal cross section of the IOP-mean RH has been prepared for the longitude belt from 150° to 160°E where the sonde data coverage over the warm pool is most plentiful (Fig. 8). At the top is shown the RH cross section computed with uncorrected data and at the bottom with HC data. Also

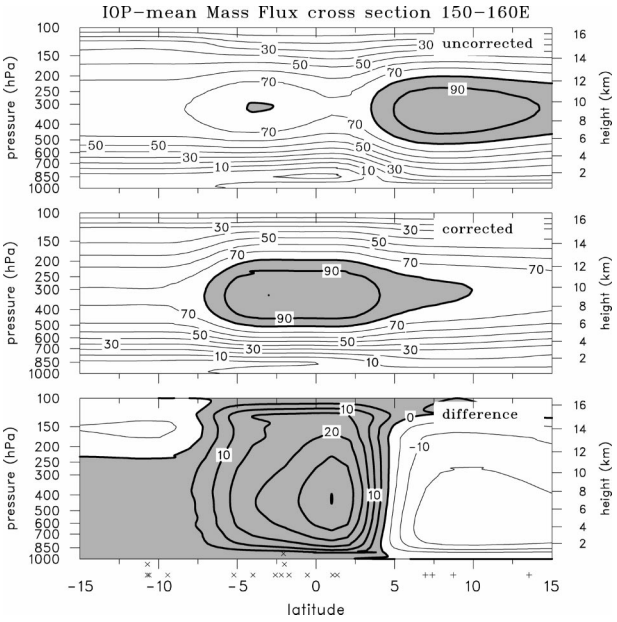

FIG. 7. IOP-mean zonally averaged convective mass flux (normalized by max value) between 150° and 160°E computed with (top) uncorrected data, (middle) corrected data, and (bottom) their difference. Values greater than 80 units are shaded (top and middle) and greater than 0 units (bottom). Symbols at the base of the bottom panel indicate the latitudes of Vaisala (×) and VIZ (+) sites used in creating this analysis.

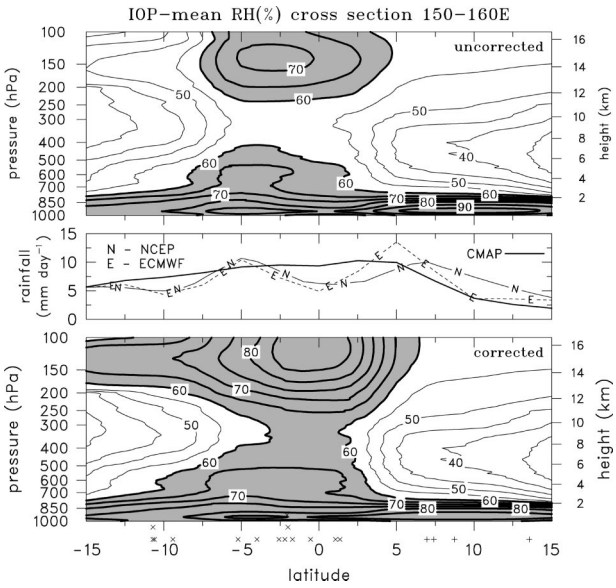

FIG. 8. IOP-mean zonally averaged relative humidity between 150° and 160°E computed with (top) uncorrected data and (bottom) HC data. Values greater than 60% are shaded. Symbols at the base of the bottom panel indicate the latitudes of Vaisala (×) and VIZ (+) sites used in creating this analysis. (middle) The IOP-mean zonally averaged rainfall rate for the same longitude band for the NCEP and ECMWF reanalyses and the CMAP rainfall product. Relative humidity was computed with respect to ice for temperatures less than 0°C.

shown in Fig. 8. (bottom) are the latitudinal locations of the sounding sites that influenced this analysis where sites with a Vaisala sensor are indicated with an ''×'' symbol and sites with VIZ sensor have a ''+'' symbol. In the uncorrected cross section, the boundary layer humidity shows a maximum over 90% in the vicinity of the VIZ sites centered around 10°N. Use of the HC data leads to a more horizontally homogeneous boundary layer moisture pattern with a maximum of 85% at nearly all latitudes north of 5°S. Also, the mid- and upper levels are moistened at the latitudes of the Vaisala sites (south of 2°N), while the midlevel dryness is readily apparent in both cross sections at the latitudes of the VIZ sites. Using a two-dimensional cloud model to study western Pacific squall lines, Lucas et al. (2000) found that increasing the moisture content above the boundary layer, particularly up to 3 km, was favorable for strengthening squall lines. Thus the moisture corrections in the boundary layer, as well as above it (as depicted in Figs. 2 and 8), will likely affect simulations of convection.

Figure 8 (middle) shows the IOP-mean rainfall averaged over the same longitude band from three sources: the NCEP and European Centre for Medium-Range Weather Forecasts (ECMWF) reanalysis products that are based on uncorrected humidity data, and the satellite-based CMAP analysis. While the CMAP analysis shows a broad maximum with a peak around 2.5°N, the reanalysis products have two peaks—one at 5°S and the other at 5°–7.5°N with a relative minimum over the latitudes of the IFA (centered around the equator). The excessive rainfall north of ~5°N and the deficit to the south in the reanalysis products follows the moisture biases depicted in the uncorrected humidity cross section. It would appear that the convective parameterizations used in the reanalysis models have translated the humidity biases into an erroneous rainfall pattern (Johnson and Ciesielski 2000). Interestingly, the changes in the convective mass flux distribution due to the HC data depicted in Fig. 7 are of the right order and sign to bring the reanalysis rainfall amounts into good agreement with the CMAP rainfall estimate. This suggests that the ECMWF and NCEP analysis products for the COARE period would benefit from a new reanalysis with the HC data.

5. Impacts on rainfall and radiative heating rate estimates

In this section we examine impacts of using the HC sonde data to diagnose rainfall and radiative heating rates from atmospheric heat and moisture budgets. A sensitivity test designed to gauge impact of the HC data will focus primarily on the IFA region, where measurements were most abundant and the analyses are most frequently used. To facilitate this testing, objective analysis of the horizontal wind components u and v, temperature T, specific humidity q (both corrected and un-

corrected), and geopotential height z at 1° horizontal resolution, 25-hPa vertical resolution were produced over the area of the LSA (10°S–10°N, 140°–180°E). These analyses were computed every 6 h for the COARE IOP using the multiquadric interpolation scheme of Nuss and Titley (1994). To assist the analysis in data-sparse regions, ECMWF reanalysis values were used along 15°N and along 180°E north of the equator at 5° intervals.

The extraction of reliable fields of divergence from sparse sounding networks such as COARE presents a formidable challenge (e.g., Ooyama 1987; Zhang and Lin 1997). In earlier versions of our gridded analyses, dipoles in the vertically averaged horizontal divergence field were observed in the vicinity of the sounding stations. Recently, Haertel (2002) concluded that these features were spurious in nature and generated by the analysis scheme. To remove this spurious divergence, a correction algorithm was developed (Haertel 2002) and applied here to the adjust the horizontal winds and divergence. Additional details of the objective analysis procedure and computation of the vertical motion (ω) field can be found in Johnson and Ciesielski (2000).

Following Yanai et al. (1973), vertical integration of the conservation laws of heat and moisture yield[6]

$$\langle Q_1 \rangle = \langle Q_R \rangle + LP + S, \tag{1}$$

$$\langle Q_2 \rangle = L(P - E), \tag{2}$$

where the apparent heat source Q_1, is defined as $c_p\{[\partial\overline{T}/\partial t + \overline{\mathbf{v}} \cdot \nabla\overline{T} + (p/p_0)^{\kappa}\overline{\omega}\partial\overline{\theta}/\partial p]\}$, and the apparent moisture sink Q_2, is defined as $-L(\partial\overline{q}/\partial t + \overline{\mathbf{v}} \cdot \nabla\overline{q} + \overline{\omega}\partial\overline{q}/\partial p)$ where $\kappa = R/c_p$, R is the gas constant, and c_p the specific heat at constant pressure for moist air, L the temperature-dependent latent heat of vaporization, $\langle Q_R \rangle$ the net radiative heating rate, P the precipitation rate, overbar denotes a horizontal average, $\langle\ \rangle \equiv 1/g \int_{p_T}^{p_s} (\ )\, dp$, p_T is the tropopause pressure, and p_s the surface pressure. Combining (1) and (2) yields

$$\langle Q_R \rangle = \langle Q_1 \rangle - \langle Q_2 \rangle - S - LE. \tag{3}$$

Our approach is to first compute the quantities of Q_1 and Q_2 with our gridded dataset, then compute precipitation P and net radiative heating $\langle Q_R \rangle$ as budget residuals from (2) and (3), respectively.

Figure 9 shows the IFA–IOP-mean vertical profiles of the apparent moisture sink computed with both the uncorrected and corrected humidity data. Use of the HC data results in an increase in Q_2, most notably at lower levels, where the apparent moistening below 925 hPa is substantially reduced. To understand why this occurs, the contributions to ΔQ_2 (i.e., the change in Q_2 due to the HC data) from the horizontal and vertical moisture advection terms are shown at the right in Fig. 9. The contribution from the moisture tendency term, $-L(\partial\overline{q}/\partial t)$, is not shown here because its impact on ΔQ_2 is negligible when averaged over the entire IOP period. The increase in Q_2 below 800 hPa is due primarily to the correction's impact on the horizontal moisture advection, $-L(\overline{\mathbf{v}} \cdot \nabla\overline{q})$, which produces less apparent moistening (or more apparent drying) over the IFA. This, in turn, can be attributed to a reduced low-level, meridional moisture gradient ($\partial\overline{q}/\partial y$ is less negative) across the latitudes of the IFA in the corrected data (Fig. 8). For example, in the uncorrected data the specific humidity averaged in the lowest 2 km decreases about 0.6 g kg^{-1} between 4°S and 1°N. In the corrected data, because sites over the northern IFA were moistened more by the correction algorithm than sites to the south, this moisture decrease is $<$0.1 g kg^{-1}. The time series of the humidity correction's impact on the horizontal advection term averaged over the IFA and the 1000–800-hPa layer (ΔQ_{2_ha}) is shown in Fig. 10 along with the corresponding time series of the IFA low-level meridional wind (v_{LL}). The high anticorrelation between these two series (-0.79) shows that horizontal advection of dry air into the IFA is reduced ($\Delta Q_{2_ha} > 0$) during periods of northerly winds ($v_{LL} < 0$) and vice versa.

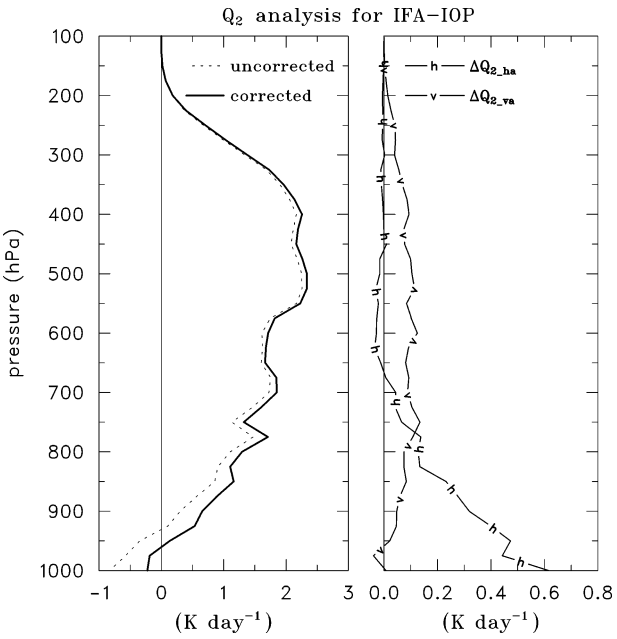

FIG. 9. IFA–IOP-mean vertical profiles of (left) apparent drying computed with humidity corrected (solid line) and uncorrected (dashed line) data, and (right) impact of the correction on the horizontal (ΔQ_{2_ha}) and vertical (ΔQ_{2_va}) moisture advection terms.

An additional, but smaller, increase in the apparent drying field results from the humidity correction's impact on the vertical advection term, $-L(\overline{\omega}\partial\overline{q}/\partial p)$. The impact on this term peaks at midlevels where the combination of a steeper vertical q gradient in the HC data

[6] The form of this equation ignores a term involving the vertical integral of the latent heat of fusion times deposition minus sublimation (Gallus and Johnson 1991).

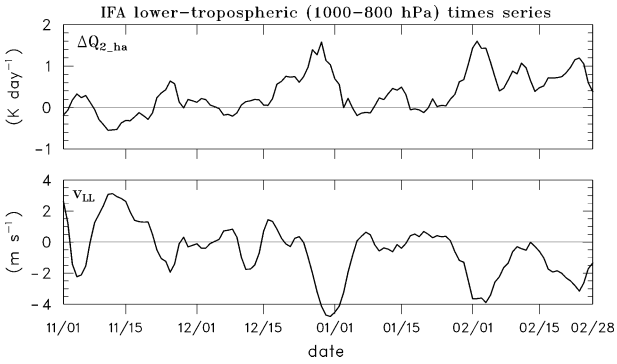

FIG. 10. Time series of analyses averaged over the IFA and the 1000–800-hPa layer: (top) the humidity correction's impact on the horizontal moisture advection term (ΔQ_{2_ha}), (bottom) the low-level meridional wind (v_{LL}).

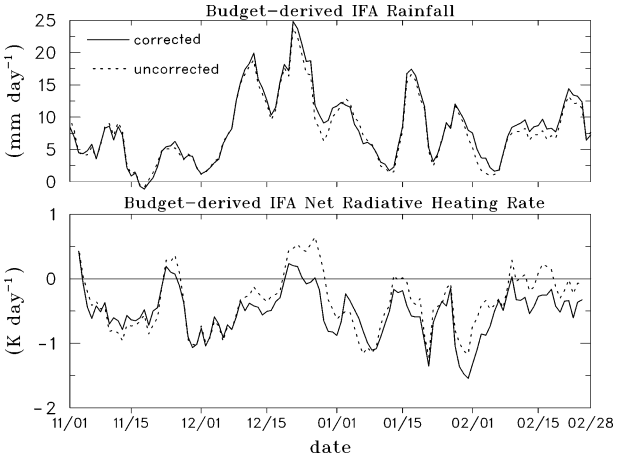

FIG. 11. Time series of (top) IFA-mean rainfall and (bottom) net radiative heating diagnosed from the atmospheric budget with corrected humidity (solid) and uncorrected (dashed) data for the COARE IOP.

Fig. 2, (middle) and the IOP-mean upward motion is a maximum. The increases in Q_2 described here have important implications for the budget-derived quantities since as seen in (2) and (3), precipitation and net radiative cooling increase as the vertical integral of Q_2 increases.

The IFA-mean time series of budget-derived precipitation and net radiative heating (computed with both corrected and uncorrected humidity data) for the COARE IOP are shown in Fig. 11. Comparing these time series to those in Fig. 10, one can see that the largest impacts from using the HC data are coincident with periods of northerly winds resulting in $\Delta Q_{2\_ha} > 0$ and enhanced apparent drying rates over the IFA. Compared to the uncorrected rainfall time series, the HC rainfall shows an improved correlation to an estimate based on the mixed satellite algorithm of Curry et al. (1999) increasing from 0.72 to 0.75 for six-hourly values (or 0.81 to 0.84 if one considers the 5-day running mean rainfall). The changes in the net radiative time series are percentagewise more substantial with enhanced cooling over extended periods. Most notably, the period of strong radiative warming near the end of December, and coincident with a strong westerly wind burst and low-level northerlies, is nearly eliminated when analyzed with HC data.

Table 3 shows the impact of using the HC data on the IFA–IOP means of the budget-derived quantities. Using the HC data increases the mean rainfall estimate by 6% to 8.42 mm day^{-1}, while the mean net radiative heating decreases by 38% to -0.55 K day^{-1}. These radiative estimates include an additional cooling of 0.05 K day^{-1} due to the effects of rain on the computation of ω, the sensible heat flux due to rain, and the frictional dissipation associated with falling rain (Johnson and Ciesielski 2000). The small differences (0.3 mm day^{-1} and 0.03 K day^{-1} for rainfall and net radiation, respectively) between the uncorrected estimates listed in Table 3 and the corresponding values cited in Johnson and Ciesielski (2000) are due to the spurious divergence correction (Haertel 2002) used in the present study. These revised values based on HC data agree well with other independent estimates of these quantities shown in Table 3.

In analyzing the radiative impact of the humidity-corrected data at R/V *Moana Wave*, Guichard et al. (2000a) found that with clear-sky conditions use of the HC data in their radiative model produces an additional net cooling of 1.29 W m^{-2} (or -0.012 K day^{-1}).[7] With partly cloudy conditions, their model produces an additional net cooling of 1.07 W m^{-2} (or -0.01 K day^{-1}) due to the HC data. These values are considerably less than our $\Delta\langle Q_R\rangle$ estimate of -0.15 K day^{-1}. It is difficult to understand the reasons for this difference, since the methods (budget residual vs direct radiative computation) are so different. One reason for this difference may be that the radiative computation of Guichard et al. (2000a) did not consider any changes in cloud cover when using humidity-corrected or uncorrected data. They acknowledge that such cloud cover changes would significantly impact their radiative computations. While beyond the scope of this study, it would be interesting to examine the radiative impact of the HC data within the context of a complete atmospheric model with interactive radiation.

Revised estimates with HC data of rainfall and net radiative heating rates for the OSA are 9.0 mm day^{-1} and -0.63 K day^{-1} for the IOP means, respectively, compared to previous estimates of 9.3 mm day^{-1} and -0.50 K day^{-1} (Johnson and Ciesielski 2000). Sensitivity tests show that the changes in the OSA estimates are due predominately to the spurious divergence correction (Haertel 2002). For this larger area the low-level drying in the corrected VIZ data has a compensating

[7] This assumes 108 W m^{-2} = -1.1 K day^{-1}.

TABLE 3. Impact of corrected humidity data on IFA–IOP means of budget-derived quantities.

	P (mm day^{-1})	$\langle Q_R \rangle$ (K day^{-1})
Uncorrected	7.91	−0.40
Change (Δ)	0.51 (+6%)	−0.15 (−38%)
Corrected	8.42	−0.55
Independent estimates	8.3 (Curry et al. 1999)	−0.38 (B. Collins, cited in Wu et al. 2000)
	9.3 (CMAP)	−0.66 (C. Long, cited in Jensen et al. 2002)
		−0.79 (Zhang and Rossow 2002)

effect on the budget quantities relative to the moistening effects of the corrected Vaisala data.

6. Impact on forcing fields for CRMs and SCMs

Yet another method for assessing the impact of the HC data is through a moist enthalpy analysis. CRMs and SCMs are forced with large-scale advective tendencies of temperature (f_T) and moisture (f_q) given by

$$f_T = -(c_{pd} + c_l q)[\mathbf{v} \cdot \nabla T + \omega(\partial T/\partial p)] + \alpha\omega$$

$$f_q = -[\mathbf{v} \cdot \nabla q + \omega(\partial q/\partial p)],$$

where c_{pd} is the specific heat capacity for dry air, c_l is the specific heat capacity of liquid water, and α is the specific volume. Predicted enthalpy K_p is a function of these forcing tendencies (Wu et al. 2000), which typically are computed from gridded objective analyses averaged over a given region. If observed enthalpy $K_o = (c_{pd} + c_l q)T + Lq$ differs significantly from K_p, then CRM and SCM simulations will develop temperature and moisture biases. Emanuel and Živković-Rothman (1999) and Wu et al. (2000) have performed a moist enthalpy analysis for the TOGA COARE period to provide some insight into the quality of the large-scale forcing data. The large-scale forcing data they used were computed from an objective analysis scheme similar to what is used in this study but with no correction for spurious divergence or humidity (Ciesielski et al. 1997). Their analysis at the end of a 120-day integration for COARE IOP showed differences between observed and predicted enthalpy ''equivalent to a 25 K temperature error integrated over the troposphere'' (Emanuel and Živković-Rothman 1999).

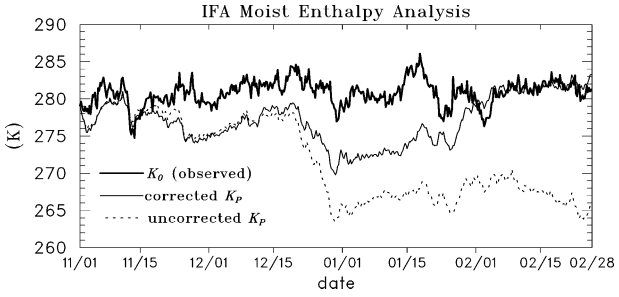

FIG. 12. Evolution of the IFA-mean, 6-hourly, vertically integrated, observed moist enthalpy (heavy solid line) and predicted enthalpy computed with humidity corrected (thin solid line) and uncorrected (dashed line) data. Following the convention of Wu et al. (2000), the vertically integrated enthalpies are divided by $c_{pd} \times 958$ hPa.

Following the procedure outlined in Wu et al. (2000) and using their radiative flux data, we repeat this moist enthalpy analysis. Figure 12 shows the observed and predicted enthalpy (computed both with and without HC data) for the COARE IOP where these quantities have been integrated over the mass of the atmosphere from the surface (1008 hPa) to 50 hPa. With K_p a function of the forcing fields, the differences between the K_p curves in Fig. 12 are related to the ΔQ_{2_ha} analysis (i.e., the HC impact on horizontal moisture advection) shown in Fig. 10. For example, the K_p curves diverge the most during periods when ΔQ_{2_ha} is most positive, as in late December and throughout much of February. In simple terms, the humidity biases lead to a spurious advection of dry air into the the IFA, which maximizes for strong meridional flow owing to the north–south distribution of VIZ–Vaisala sites and their biases. The cumulative effect of this error over many days leads to a larger enthalpy drift. At the end of the 120-day integration the difference between K_p and K_o with uncorrected humidity data is about 15 K; with HC data the difference is only a few degrees.[8] This suggests that a model simulation of the entire IOP forced with the HC data would exhibit less of an enthalpy trend than one forced with the uncorrected data.

7. Impact on the diurnal cycle

Wang et al. (2002) noted that four island VaH sites (Kapinga, Kavieng, Manus, and Nauru) have a significantly larger correction during the daytime. While the reasons for this day–night difference are still being investigated, we consider here how the corrected humidities affect the diurnal cycle over the IFA. The diurnal variation of the correction's impact on boundary layer specific humidity ($\Delta q_{\rm bl}$) is shown in the Fig. 13 (top). Consistent with Wang et al., $\Delta q_{\rm bl}$ shows a larger increase in moisture occurs during the daylight hours (1000 and 1600 LT). Above the boundary layer, no significant diurnal variation in Δq is observed.

With positive Δq at all hours one might also expect increased rainfall (due to increased Q_2) and from (3) de-

[8] The spurious divergence correction accounts for the smaller 120-day entropy trend of 15 K compared to the 25 K found by Emanuel and Živković-Rothman (1999) and Wu et al. (2000).

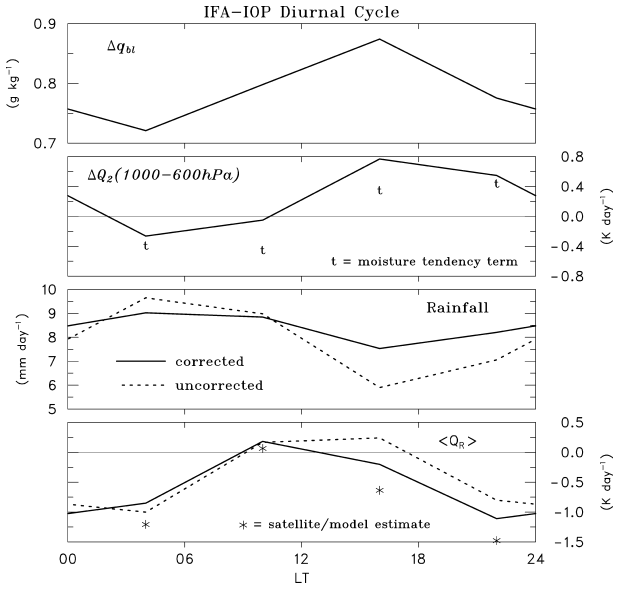

FIG. 13. Diurnal cycle of IFA–IOP-mean fields. (top) Change in boundary layer specific humidity (Δq_{BL}) due to the humidity correction; (middle upper) change in lower-tropospheric (1000–600 hPa) apparent drying (ΔQ_2) due to the humidity correction where the t symbols show the contribution to ΔQ_2 due to the tendency term; (middle lower) budget-derived rainfall computed with humidity corrected (solid line) and uncorrected (dashed line) data; (bottom) budget-derived net radiative heating computed with humidity corrected (solid line) and uncorrected (dashed line) data. Also denoted by the star symbols (*) in the bottom panel are satellite/model estimates of net radiative heating from Zhang and Rossow (2002).

creased $\langle Q_R \rangle$ at all hours. Instead, the change in the diurnal variation of these fields is more complex. A significant rainfall increase and $\langle Q_R \rangle$ decrease is observed at 1600 and 2200 LT with a weaker but opposite trend at 0400 and 1000 LT (bottom two panels of Fig. 13). The primary reason for this follows directly from the larger daytime moisture correction, as noted earlier, which affects the local moisture tendency term ($-L\partial q/\partial t$). This tendency term, which is generally small in magnitude compared to the advection terms, can significantly impact the moisture budget on a diurnal timescale. In the second panel of Fig. 13 one can see that the diurnal changes in the Q_2 field due to the humidity correction (ΔQ_2), are largely determined by changes in the tendency term (indicated with a t symbol) showing a moistening effect (t, $\Delta Q_2 < 0$) at 0400 and 1000 LT and a drying effect (t, $\Delta Q_2 > 0$) at 1600 and 2200 LT. The remaining difference seen here between ΔQ_2 and the tendency term is due primarily to the diurnal variation of ΔQ_{2_ha} (not shown), which is positive at all hours but largest at 1000 and 1600 LT. Given this diurnal variation of ΔQ_2 and the direct proportionality of $\langle Q_2 \rangle$ to P and $-\langle Q_R \rangle$ in budget Eqs. (2) and (3), one can readily see how the HC data impacts diurnal changes in rainfall and net radiative heating (bottom two panels of Fig. 13, respectively).

The main impact of using the HC data is a reduction in the amplitude of the diurnal rainfall variation by increasing the rainfall amount at 1600 and 2200 LT. With the caveat that resolving diurnal features with 6-hourly observations is difficult and results inconclusive, we offer the following comparisons with other studies. The early morning maximum in budget-derived rainfall is consistent with radar analysis of Short et al. (1997), which covered a region about half the size of the IFA and was available for 101 days of the 120 day IOP. Their radar analysis also showed a 1000 LT minimum in rainfall and a secondary afternoon maximum. While the afternoon increase in rainfall computed with the HC data may be an improvement in terms of capturing the afternoon secondary maximum observed by radar, the 6-hourly budget analysis is unable to resolve neither this maximum precisely nor the 1000 LT rainfall minimum detected by the radar. Use of the HC data increases the net radiative cooling rate at 1600 and 2200 LT with little impact at other hours, resulting in a diurnal variation in better agreement with an independent estimate (denoted by the * symbols in Fig. 13; Zhang and Rossow 2002). The impact is particularly large at 1600 LT where the uncorrected data show a net warming of 0.24 K day^{-1}, while the corrected data show a net cooling of -0.20 K day^{-1}.

8. Summary and concluding remarks

Due to the importance of the TOGA COARE upper-air sounding dataset, ongoing efforts have continued to improve its quality. This study investigates the impacts of the humidity-corrected (HC) dataset, released by NCAR/ATD, on various analyses over the LSA domain of COARE. This dataset contains corrected humidity for 42 sounding sites in the COARE domain, which includes both Vaisala and VIZ systems. The nature of the Vaisala humidity errors, which come from six sources, is discussed in detail in Wang et al. (2002). This study describes the correction procedure for the VIZ humidity errors. The humidity corrections, which are largest in the lower-tropospheric levels, generally increase the moisture in the Vaisala sondes and decrease it in the VIZ sondes.

Because of the sensitivity of convection to low-level thermodynamic properties, use of the HC data gives one a much different perspective on the characteristics of convection during TOGA COARE. For example, the moisture increase in the HC VaH sondes, launched primarily from sites in the IFA, increases the IOP-mean value of CAPE by 450 J kg^{-1} and decreases |CIN| by 96 J kg^{-1}. Opposite trends in these parameters are observed at the VIZ sites that lie along the northern edge of the LSA. With uncorrected data, the difference in the IOP-mean CAPE between the VaH and VIZ sites is over 750 J kg^{-1}; after correction both CAPEs are $\sim$1300 J kg^{-1}, which is consistent with a generally uniform SST field over the warm pool.

Application of the HC data in a 1D cloud model shows that convective mass fluxes in the 500–300-hPa

layer increase ~30% for the VaH sites near the equator and decrease ~15% at the VIZ sites near 10°N. These results suggest that the intensity and location of convection would be significantly different in model simulations that use the HC data. Using uncorrected data one might mistakenly conclude that convection is difficult to trigger over the IFA and overly primed for vigorous convection at the VIZ sites to the north. Use of the HC data gives a more realistic view of the atmosphere's convective potential and its spatial distribution over a warm pool region. In addition, we have noted the difficulty that the reanalysis products had in reproducing the rainfall pattern observed during COARE—a likely consequence of the humidity instrument biases. For this reason, we believe that the reanalysis products for the COARE period could be improved with a new reanalysis using the corrected humidity data.

Use of the HC data appears to have a beneficial impact on budget-derived estimates. The IFA–IOP-mean rainfall diagnosed as a budget residual increases by 6% (from 7.91 to 8.42 mm day^{-1}) due to the HC data. A more substantial change is observed in the IFA–IOP mean of net radiative heating, which decreases by 38% (from -0.40 to -0.55 K day^{-1}) from using the HC data. These new estimates based on the HC data are in better agreement with those from other independent sources.

We also examined the impact of the HC data in terms of a moist enthalpy analysis. Such analysis has been used by previous investigators to evaluate the quality of the large-scale forcing data for CRM and SCM simulations. Our analysis suggests that model simulations of the entire IOP forced with HC data will exhibit substantially smaller enthalpy trends than simulations forced with uncorrected data.

The efforts invested to correct the sonde humidity data have gone a long way towards improving the quality of the humidity field for COARE. Unfortunately some errors still remain. The most notable problems in the HC dataset that we are aware of include: 1) a significant moist bias in the R/V *Kexue 1* sonde data still exists and appears to have gotten worse in the ''corrected'' dataset, 2) the original humidity data from the R/V *Vickers* is judged to be of good quality, whereas the correction scheme appears to dry the sondes too much, 3) use of the R/V *Moana Wave* humidity data in a study of the mixed layer over the warm pool suggests that it may have been slightly undercorrected (i.e., not moistened enough), and 4) no corrections have been made to the VIZ sondes above 700 hPa. Despite these lingering issues, the improvements already made to the TOGA COARE upper-air sonde dataset make it one of the highest quality tropical sonde datasets ever collected.

Based on the comparison of several analyses with and without the humidity corrections, we contend that the HC dataset described herein has resulted in a much improved large-scale analysis of the water vapor field for the COARE IOP. These improvements should lead to more accurate simulations of convection and large-scale circulations in global models, as well as in CRMs and SCMs. To encourage the use of this improved dataset, our gridded LSA analyses and IFA-mean large-scale forcing dataset computed with the HC data, as described in this paper, have been made available at http://tornado.atmos.colostate.edu/togadata/.

Acknowledgments. This research has been supported by the NOAA Project NA67RJ0152. We commend the efforts of Ed Zipser whose persistence in calling attention to the humidity errors in the TOGA COARE sonde data ultimately lead to their correction. Special thanks go to Drs. Paquita Zuidema and Brian Mapes for providing us with the code for the buoyancy-sorting cloud model and for their patience in helping us use it, to Xiaoqing Wu for furnishing us with the radiative flux data used in the moist enthalpy analysis, to Yuanchong Zhang and Bill Rossow for making available their latest radiative estimates for the COARE period, and for the assistance of Rick Taft in developing the code for the multiquadric interpolation scheme.

REFERENCES

Ciesielski, P. E., L. M. Hartten, and R. H. Johnson, 1997: Impacts of merging profiler and rawinsonde winds on TOGA COARE analyses. *J. Atmos. Oceanic Technol.,* **14,** 1264–1279.

Crook, N. A., 1996: Sensitivity of moist convection forced by boundary layer processes to low-level thermodynamic fields. *Mon. Wea. Rev.,* **124,** 1757–1785.

Curry, J. A., C. A. Clayson, W. B. Rossow, R. Reeder, Y.-C. Zhang, P. J. Webster, G. Liu, and R.-S. Sheu, 1999: High-resolution satellite-derived dataset of the surface fluxes of heat, freshwater, and momentum for the TOGA COARE IOP. *Bull. Amer. Meteor. Soc.,* **80,** 2059–2080.

Elliott, W. P., and D. J. Gaffen, 1991: On the utility of radiosonde humidity archives for climate studies. *Bull. Amer. Meteor. Soc.,* **72,** 1323–1326.

Emanuel, K. A., and M. Živković-Rothman, 1999: Development and evaluation of a convection scheme for use in climate models. *J. Atmos. Sci.,* **56,** 1766–1782.

Ferrier, B. S., and R. A. Houze Jr., 1989: One-dimensional time dependent modeling of GATE cumulonimbus convection. *J. Atmos. Sci.,* **46,** 330–351.

Gallus, W. A., Jr., and R. H. Johnson, 1991: Heat and moisture budgets of an intense midlatitude squall line. *J. Atmos. Sci.,* **48,** 122–146.

Guichard, F., D. Parsons, and E. Miller, 2000a: Thermodynamic and radiative impact of the correction of sounding humidity bias in the Tropics. *J. Climate,* **13,** 3611–3624.

——, J. L. Redelsperger, and J. P. Lafore, 2000b: Cloud-resolving simulation of convective activity during TOGA-COARE: Sensitivity to external sources of uncertainties. *Quart. J. Roy. Meteor. Soc.,* **126,** 3067–3096.

Gutzler, D. S., 1993: Uncertainties in climatological tropical humidity profiles: Some implications for estimating the greenhouse effect. *J. Climate,* **6,** 978–982.

Haertel, P. T., 2002: Spurious divergence within objective analyses with application to TOGA COARE heat and moisture budgets. Preprints, *25th Conf. on Hurricanes and Tropical Meteorology,* San Diego, CA, Amer. Meteor. Soc., 192–195.

Jensen, M. P., T. P. Ackerman, and S. M. Sekelsky, 2002: Radiative

impacts of anvil cloud during the Maritime Continent Thunderstorm Experiment. *J. Appl. Meteor.,* **41,** 473–487.

Johnson, R. H., and P. E. Ciesielski, 2000: Rainfall and radiative heating rates from TOGA COARE atmospheric budgets. *J. Atmos. Sci.,* **57,** 1497–1514.

——, ——, and K. A. Hart, 1996: Tropical inversions near the 0° level. *J. Atmos. Sci.,* **53,** 1838–1855.

——, ——, and J. A. Dickey, 2001: Multiscale variability of the atmospheric mixed layer over the western Pacific warm pool. *J. Atmos. Sci.,* **58,** 2729–2750.

LeMone, M., E. Zipser, and S. Trier, 1998: The role of environmental shear and thermodynamic conditions in determining the structure and evolution of mesoscale convective systems during TOGA COARE. *J. Atmos. Sci.,* **55,** 3493–3518.

Lin, X., and R. H. Johnson, 1996: Heating, moistening, and rainfall over the western Pacific warm pool during TOGA COARE. *J. Atmos. Sci.,* **53,** 3367–3383.

Loehrer, S. M., T. A. Edmands, and J. A. Moore, 1996: TOGA COARE upper-air sounding data archive: Development and quality control procedures. *Bull. Amer. Meteor. Soc.,* **77,** 2651–2671.

Lucas, C., and E. J. Zipser, 2000: Environmental variability during TOGA COARE. *J. Atmos. Sci.,* **57,** 2333–2350.

——, ——, and B. S. Ferrier, 2000: Sensitivity of tropical west Pacific oceanic squall lines to tropospheric wind and moisture profiles. *J. Atmos. Sci.,* **57,** 2351–2373.

Mapes, B. E., and R. A. Houze Jr., 1992: An integrated view of the 1987 Australian monsoon and its mesoscale convective systems. Part I: Horizontal structure. *Quart. J. Roy. Meteor. Soc.,* **118,** 927–963.

Nicholls, M. E., R. H. Johnson, and W. R. Cotton, 1988: The sensitivity of two-dimensional simulations of tropical squall lines to environmental profiles. *J. Atmos. Sci.,* **45,** 3625–3649.

Nuss, W. A., and D. W. Titley, 1994: Use of multiquadric interpolation for meteorological objective analysis. *Mon. Wea. Rev.,* **122,** 1611–1631.

Ooyama, K., 1987: Scale-controlled objective analysis. *Mon. Wea. Rev.,* **115,** 2476–2506.

Parsons, D., K. Yoneyama, and J.-L. Redelsperger, 2000: The evolution of the tropical western Pacific atmosphere–ocean system following the arrival of a dry intrusion. *Quart. J. Roy. Meteor. Soc.,* **126,** 517–548.

Raymond, D. J., 1995: Regulation of moist convection over the west Pacific warm pool. *J. Atmos. Sci.,* **52,** 3945–3959.

——, A. M. Blyth, 1992: Extensions of the stochastic mixing model to cumulonimbus clouds. *J. Atmos. Sci.,* **49,** 1968–1983.

Sherwood, S. C., 1999: Convective precursors and predictability in the tropical western Pacific. *Mon. Wea. Rev.,* **127,** 2977–2991.

Short, D. A., P. A. Kucera, B. S. Ferrier, J. C. Gerlach, S. A. Rutledge, and O. W. Thiele, 1997: Shipboard radar rainfall patterns within the TOGA COARE IFA. *Bull. Amer. Meteor. Soc.,* **78,** 2817–2836.

Soden, B. J., and J. R. Lanzante, 1996: An assessment of satellite observations and model simulations of upper-tropospheric humidity. *J. Climate,* **9,** 1235–1250.

Spencer, R. W., and W. D. Braswell, 1997: How dry is the tropical free troposphere? Implications for global warming theory. *Bull. Amer. Meteor. Soc.,* **78,** 1097–1106.

Wade, C. G., and B. Schwartz, 1993: Radionsonde humidity observations near saturation. Preprints, *Eighth Symp. on Meteorological Observations and Instrumentation,* Anaheim, CA, Amer. Meteor. Soc., 44–49.

Wang, J., H. L. Cole, D. J. Carlson, E. R. Miller, K. Beierle, A. Paukkunen, and T. K. Laine, 2002: Corrections of humidity measurement errors from the Vaisala RS80 radiosonde—Application to TOGA COARE data. *J. Atmos. Oceanic Technol.,* **19,** 981–1002.

Webster, P. J., and R. Lukas, 1992: TOGA COARE: The Coupled Ocean–Atmosphere Response Experiment. *Bull. Amer. Meteor. Soc.,* **73,** 1377–1416.

Wu, X., M. W. Moncrieff, and K. A. Emanuel, 2000: Evaluation of large-scale forcing during TOGA COARE for cloud-resolving models and single-column models. *J. Atmos. Sci.,* **57,** 2977–2985.

Xie, P., and P. A. Arkin, 1997: Global precipitation: A 17-year monthly analysis based on gauge observations, satellite estimates, and numerical model output. *Bull. Amer. Meteor. Soc.,* **78,** 2539–2558.

Yanai, M., S. Esbensen, and J. H. Chu, 1973: Determination of bulk properties of tropical cloud clusters from large-scale heat and moisture budgets. *J. Atmos. Sci.,* **30,** 611–627.

Zhang, M. H., and J. L. Lin, 1997: Constrained variational analysis of sounding data based on column-integrated conservations of mass, heat, moisture, and momentum: Approach and application to ARM measurements. *J. Atmos. Sci.,* **54,** 1503–1524.

Zhang, Y.-C., and W. B. Rossow, 2002: New ISCCP global radiative flux data products. *GEWEX News,* Vol. 12, No. 4, International GEWEX Project Office, 7.

Zipser, E. J., and R. H. Johnson, 1998: Systematic errors in radiosonde humidities: A global problem? Preprints, *10th Symp. on Meteorological Observations and Instrumentation,* Phoenix, AZ, Amer. Meteor. Soc., 72–73.

Zuidema, P., 1998: The 600–800-mb minimum in tropical cloudiness observed during TOGA COARE. *J. Atmos. Sci.,* **55,** 2220–2228.